

# On the interplay of friction and stress relaxation to improve stretch-flangeability of dual phase (DP600) steel

Kali Prasad<sup>a</sup>, Venkatesh B<sup>c</sup>, Hariharan Krishnaswamy<sup>a,\*</sup>, Dilip K Banerjee<sup>b</sup>, Uday Chakkingal<sup>c</sup>

<sup>a</sup>*Manufacturing Engineering Section, Department of Mechanical Engineering, IIT Madras, Chennai-600036, India*

<sup>b</sup>*Material Measurement Laboratory, National Institute of Standards and Technology(NIST), Gaithersburg, Maryland 20899, USA*

<sup>c</sup>*Metal Forming Laboratory, Department of Metallurgical and Materials Engineering, IIT Madras, Chennai-600036, India*

---

## Abstract

Industrial servo presses have been used to successfully demonstrate improved formability when deforming sheet metals. While the time dependent viscoplastic behavior of material is attributed to the observed formability improvement, much less effort has been devoted to understand and quantify the underlying mechanisms. In this context, the hole expansion test (HET) of a dual phase steel was interrupted at pre-defined punch travel heights to understand the time-dependent effects on stretch-flangeability. The effect of pre-strain, hold time and edge quality on hole expansion ratio (HER) improvement was studied. The present study shows that the HER improves significantly in interrupted HET. This improved HER is due to the combined effects of stress relaxation and friction on deformation behavior. The ductility improvement estimated from uniaxial stress relaxation tests was used to estimate the contribution of stress relaxation and friction, respectively, in HET. This study shows that friction plays a significant role in improving HER at high pre-strain. It was also demonstrated that frictional effects are largely influenced by edge quality.

*Keywords:* Stretch-flangeability, Hole expansion ratio, Dual phase steel Stress relaxation, Servo press, Finite element analysis

---

\*Corresponding author

*Email addresses:* kali.iitm@gmail.com (Kali Prasad), venkateshmme4@gmail.com (Venkatesh B), hariharan@iitm.ac.in (Hariharan Krishnaswamy), dilip.banerjee@nist.gov (Dilip K Banerjee), udaychak@iitm.ac.in (Uday Chakkingal)

## 1. Introduction

Dual phase (DP) steels belong to the family of first generation advanced high strength steels (AHSS), which have a microstructure exhibiting two distinct phases, namely ferrite and martensite [1, 2]. DP steels, known for their excellent combination of strength and ductility, exhibit poor stretch-flangeability [3, 4]. Stretch flangeability refers to the ability of the material to resist edge cracking during sheet metal forming operations [5]. In a typical sequence of multistage forming of sheet components, flanging is performed toward the later stages after large plastic strain and significant work hardening take place [6, 7]. Stretch-flangeability can be evaluated with the HET, where a circular blank with a central hole is deformed using a rigid punch. The central hole expands and the test is continued until the failure of sheet is indicated by the appearance of surface cracks. The ratio of the change in the initial hole diameter to the initial hole diameter estimated from HET is referred as the HER and is used to quantify the stretch-flangeability of the material [8]. Higher values of HER indicate better stretch-flangeability. The central hole of a standard HET specimen is usually punched, although other methods such as drilling, shearing, wire cut electrical discharge machining (EDM), laser trimming and reaming [3, 9, 10] have been used in the past. The HER estimated is highly sensitive to the process used for hole preparation due to the edge condition [11–13]. For instance, micro-cracks that typically form at the end machining step can possibly serve as damage initiation sites [3, 14, 15] during HET. This is further confirmed by the correlation between fracture toughness and HET as reported in literature [13, 16, 17]. The good correlation of HER prediction with damage models for different materials (microstructure) further proves that the edge condition rather than base microstructure plays a dominant role in determining the final HER values. Hole expansion occurs in routine forming operations. A traditional forming limit diagram (FLD) is not suitable for predicting edge cracking during stretching operations as failure is sensitive to the edge condition [3, 18]. In general, sheets with finished holes perform better than those with sheared edges. HER estimate is strain path dependent, as evident from its variation with punch geometry. It was shown that the failure region is subjected to a uniaxial state of stress when a conical punch is used and a plane strain state when a flat bottom punch is used [3, 19]. The state of stress is complex and varies continuously with deformation when using a hemispherical punch [19].

33 In addition to the effects of edge condition and punch shape, HER is dependent on  
34 the metallurgical parameters such as non-metallic inclusions [20], grain size [21, 22] and  
35 microstructure [23]. The relative strength difference between the soft ferrite and hard  
36 martensite plays an important role on the edge formability of DP steels [23, 24]. Fang  
37 et al.[23] investigated the effect of tempering temperature on hole expansion behavior of  
38 C-Mn steel and found that the HER increased after tempering due to the reduction of  
39 strength difference between ferrite and martensite phases.

40 As discussed above, HER is influenced by edge quality and loading path, in addition  
41 to microstructure. Therefore, for a given material (microstructure) HER can be improved  
42 by modifying the deformation process parameters and edge preparation. Although many  
43 attempts have been made to relate HER with tensile properties such as ultimate tensile  
44 strength (UTS) and uniform elongation, HER was found to correlate well with fracture  
45 strain or fracture toughness [13, 15, 25]. The onset of fracture during sheet metal  
46 forming can be postponed using non-conventional forming processes such as the servo  
47 press [26, 27]. The stepped punch travel using a servo press is known to improve the  
48 formability of sheet metals [26, 28, 29]. Altan and coworkers [30] have demonstrated that  
49 HER can be improved using servo press technology. Although the exact mechanism for  
50 formability improvement using a servo press is not yet established, it is believed that stress  
51 relaxation phenomena [31] play an important role, while effects of other factors related to  
52 friction cannot be ignored. Controlled uniaxial stress relaxation tests have shown ductility  
53 improvement <sup>1</sup> in many alloys [32–35]. As mentioned earlier, the formability improvement  
54 when using a servo press could result from multiple factors including stress relaxation,  
55 strain path change and transient contact conditions. It is challenging to separate the  
56 contribution of each of these factors in deciphering the formability improvement using  
57 servo press. Since a uniaxial stress state exists at the edge condition of HET when using  
58 conical punch, a uniaxial test is expected to provide valuable insights on the role of other  
59 factors without the complications arising from multi-axial stress states and strain path  
60 changes.

61 In the present work, systematic investigation of stretch-flangeability in DP600 steel  
62 was performed. The first objective of the study is to determine the effect of stress

---

<sup>1</sup>Ductility in this manuscript refers to uniform elongation, unless otherwise stated

63 relaxation on the hole expansion behavior of DP600. Standard hole expansion tests  
64 were conducted in two different test modes: (i) monotonic and (ii) interrupted. The  
65 latter mode can be used to correlate with uniaxial stress relaxation tests. Finite  
66 element simulation of HET is carried out to estimate the average strain rate at the  
67 hole edge where uniaxial stress state exists. The estimated strain rate is used to  
68 conduct uniaxial stress relaxation experiments. Single step stress relaxation experiments  
69 were conducted to study the influence of pre-strain and relaxation time on ductility  
70 improvement. The uniaxial tensile deformation was correlated with HER results. The  
71 second objective of the investigation is to quantify the contribution of stress relaxation  
72 on hole expansion behavior of DP600 using analysis of uniaxial stress relaxation tests.  
73 A detailed microstructural analyses of the failed samples after HET was also conducted  
74 using a scanning electron microscope.

## 75 2. Materials and Methods

76 The material used in the present work is hot rolled, pickled and oiled (HRPO) DP600  
77 sheet with thickness 2.6 mm, obtained from ArcelorMittal <sup>2</sup>. The chemical composition  
78 of as received DP600 steel was measured using Optical Emission Spectroscopy (OES) and  
79 is listed in Table:A.8.

Table 1: Chemical composition of as-received DP600 steel (mass fraction %).

Elements	C	Si	Mn	Cr	Ni	Al	S	P	Fe
Contents(%)	0.08	0.13	0.94	0.57	0.017	0.03	0.005	0.039	balance

### 80 2.1. Uniaxial mechanical testing

81 Monotonic and stress relaxation tests were conducted using a Zwick Roell Z100  
82 100 kN universal tensile testing machine equipped with an optical non contact video  
83 extensometer. Tensile specimens were prepared as per the ASTM E8 standard [36].  
84 Stress relaxation tests were conducted by stopping the machine without unloading the

---

<sup>2</sup>Certain commercial equipment, instruments, software or materials are identified to describe a procedure or concept adequately. Such identification is not intended to imply recommendation, endorsement or implication by NIST that the equipment, instruments, software or materials identified are necessarily the best available for the purpose.

85 specimen at a pre-defined strain for a known relaxation time. The tensile test was resumed  
 86 post relaxation in the initial strain rate until fracture. Details of monotonic and stress  
 87 relaxation experiments are tabulated in Table 2. All the experiments were repeated three  
 88 times.

Table 2: Experimental parameters used in uniaxial stress relaxation study.

Test mode	Strain rate ( $s^{-1}$ )	Interruption strain (% UTS)	Time (s)
Monotonic	0.042	-	-
Interrupted	0.042	50	60
		70	10
		70	60

## 89 2.2. Hole expansion test

90 HET were performed on  $90 \times 90$  mm<sup>2</sup> square sheets with a centre hole of diameter  
 91 10 mm using a conical punch with a cone angle of 60°. Central hole was prepared using  
 92 drilling and boring process. Both the hole preparation techniques involved two stages.  
 93 In the case of drilled hole, a 5 mm diameter central hole was drilled followed by 10 mm  
 94 diameter drilling at 630 rpm. In the case of bored hole, 9.5 mm central hole was drilled  
 95 followed by boring at 500 rpm using a single point boring tool. The lip angle of the drill  
 96 bits used was 59°. Both the above process were performed in a vertical drilling machine  
 97 (HMT - TRM 3V). Standard laboratory deburring technique using abrasive papers were  
 98 used to remove the visible burrs. The deburring was limited to treating visible burrs so  
 99 as to maintain the surface roughness during further processing.

100 A blank holder force of 65 kN was applied to hold the blank and prevent draw-in of  
 101 the sheet. A video camera with a light source was used to record the images of the edge  
 102 as the hole expanded and was viewed on a computer monitor. Testing was stopped on the  
 103 visual detection of a through-thickness crack. HET was conducted as per the ISO 16630  
 104 2009 standard (Figure.1). In the present study, experiments (Figure.2) were conducted  
 105 in two different modes (i) monotonic mode (punch continuously deforms the blank) (ii)  
 106 interrupted mode, where the punch was stopped intermittently during the test. The hole  
 107 expansion ratio (HER) value was calculated using equation (1).

$$HER(\%) = \frac{d_f - d_o}{d_o} \times 100 \quad (1)$$

108 where,  $d_f$  and  $d_o$  represents the final and initial diameter of the central hole.  $d_o$  is  
 109 calculated using the average value of four diameters measured at angles of  $45^\circ$ .

110 The ductility improvement due to stress relaxation is sensitive to pre-strain, strain  
 111 rate and hold time [33, 34]. In practice, punch travel can be correlated with the pre-strain  
 112 in the sample. Two different punch displacement positions, 50% and 70% of maximum  
 113 punch travel were chosen arbitrarily to perform interrupted HET. It was recently shown  
 114 that [35] at room temperature, relaxation time greater than 60 s does not enhance the  
 115 ductility significantly. Therefore, the holding time was limited to 60 s. In a typical  
 116 production set up, holding time should be as minimum as possible to maximize the  
 117 throughput. Hence a lower range of 10 s was used to quantify the contribution of stress  
 118 relaxation on hold time. The experimental conditions of monotonic and interrupted HET  
 119 are given in Table 3. Each test condition was repeated thrice and the average values along  
 120 with standard deviations are reported.

121 Equivalent failure strains in HET were estimated using analytical equations developed  
 122 by Butcher et al.[37] by measuring the inner hole diameter ( $d_{inner}$ ), outer hole diameter  
 123 ( $d_{outer}$ ) and sheet thickness around the circumference at failure ( $t_{edge}$ ):

$$\epsilon_{eq} = \frac{2}{3}(\epsilon_c - \epsilon_t) \quad (2)$$

where,  $\epsilon_c$  and  $\epsilon_t$  are circumferential and thickness, strain given by

$$\epsilon_c = \ln \left( \frac{d_{outer} + d_{inner}}{2d_o} \right)$$

$$\epsilon_t = \ln \left( \frac{t_{edge}}{t_o} \right)$$

124 where,  $d_o$  and  $t_o$  are initial hole diameter and sheet thickness respectively.

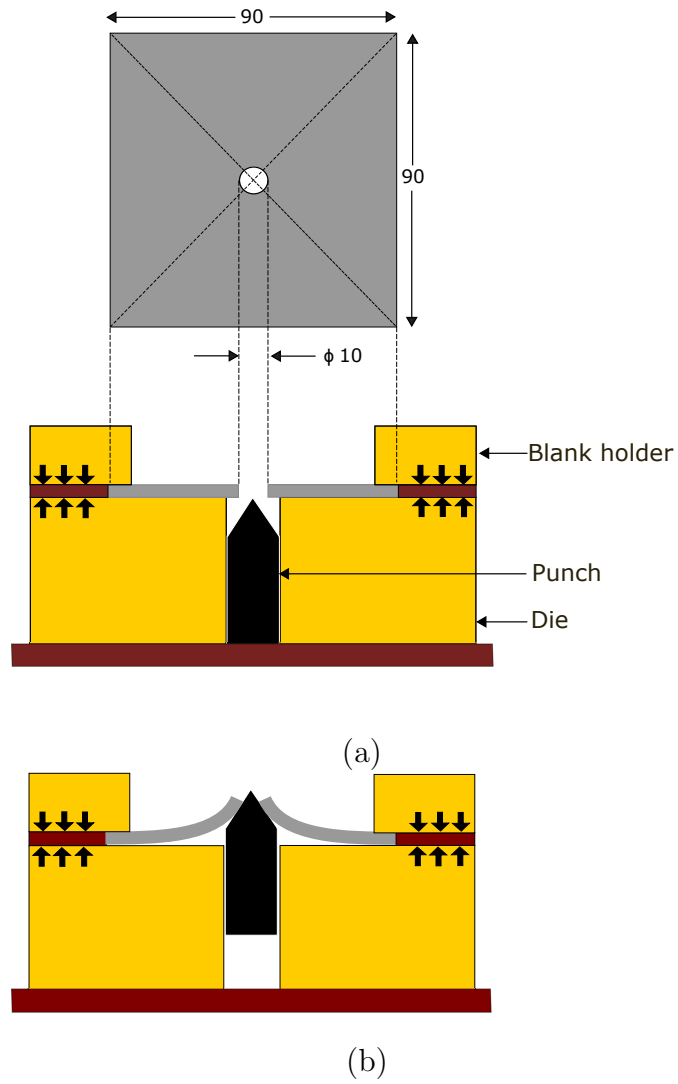


Figure 1: A schematic diagram of the hole expansion test(a) before the test, and (b) after test completion.(All the dimensions are in mm)

Table 3: Experimental parameters used in hole expansion tests.

Edge condition	Test mode	Interruption (% Punch travel)	Hold time(s)
Drilled edge	Monotonic	-	-
	Interrupted	50	60
	Interrupted	70	10
	Interrupted	70	60
Bored edge	Monotonic	-	-
	Interrupted	50	60
	Interrupted	70	10
	Interrupted	70	60

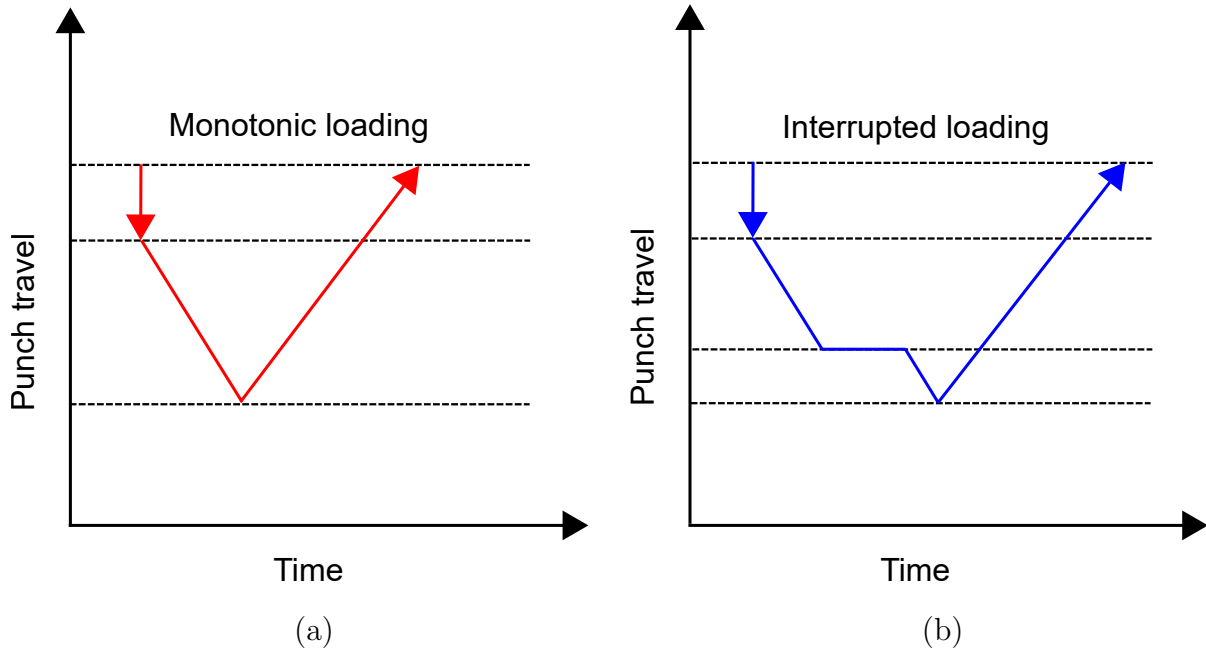


Figure 2: Schematic diagram illustrating loading path in (a) monotonic HET and (b) interrupted HET

125 *2.3. Finite element simulation of HET tests*

126 Finite element analysis was performed using commercially available ABAQUS  
 127 \Explicit 6.14 software. The conical punch was modelled as an analytically rigid body.  
 128 The  $90 \times 90 \text{ mm}^2$  rectangular blank with a central hole of 10 mm diameter and thickness  
 129 of 2.6 mm was modelled as a deformable material. The rectangular blank was meshed  
 130 using three dimensional continuum elements (C3D8R) with progressively finer mesh near

131 the hole region. The through-thickness direction of the blank was meshed with at least  
 132 10 elements considering the large local bending deformation. The contact between tool  
 133 and blank was modelled assuming Coulomb friction with a coefficient of 0.2 [10]. The  
 134 punch was constrained to move only in the vertical direction with a constant velocity of  
 135 10 mm/min. The edges of the blank were completely constrained for displacement and  
 136 rotation. The mechanical behavior of the blank was assumed to follow the von Mises  
 137 yield criterion, as the equivalent strain estimated for HET using equation (Eq.2) is valid  
 138 only for isotropic materials. Finite element simulations performed did not show any  
 139 measurable difference in the strain distribution (refer Appendix A) between von Mises  
 140 and anisotropic Hill 48 yield criteria. Therefore, anisotropy of mechanical properties due  
 141 to crystallographic texture was ignored in the present simulation. The strain hardening  
 142 behavior of the material was modelled using the hybrid hardening law as in eq.3. The  
 143 hybrid hardening law has been successfully used to describe the mechanical behavior  
 144 including in the post necking region [38].

$$\sigma = \sigma_0 + zK\epsilon_p^n + (1 - z)C(1 - e^{-\alpha\epsilon_p}) \quad (3)$$

145 Where,  $\sigma_0$  is yield stress,  $\epsilon_p$  is plastic strain,  $C$ ,  $\alpha$ ,  $K$ ,  $n$  are material constants and  $z$  is  
 146 the weight factor ( $0 \leq z \leq 1$ ) that is used to combine Swift and Voce hardening laws. The  
 147 parameters of the combined Swift-Voce isotropic hardening law were obtained by least  
 148 square fitting of the experimental true stress-true plastic strain data of uniform elongation  
 149 from the uniaxial tensile tests. The weight factor,  $z$ , was estimated by fitting the post  
 150 necking behavior of similar materials in literature [38]. Figure.3. shows the extrapolated  
 151 true stress and true plastic strain data using this hybrid hardening law. The values of  
 152 fitted parameters of the hardening model are tabulated in Table 4.

Table 4: Fitting parameters of the combined Swift-Voce strain hardening law.

$\sigma_0$	$z$	$K$	$n$	$C$	$\alpha$
400	0.74	623.5	0.45	640.7	34.65

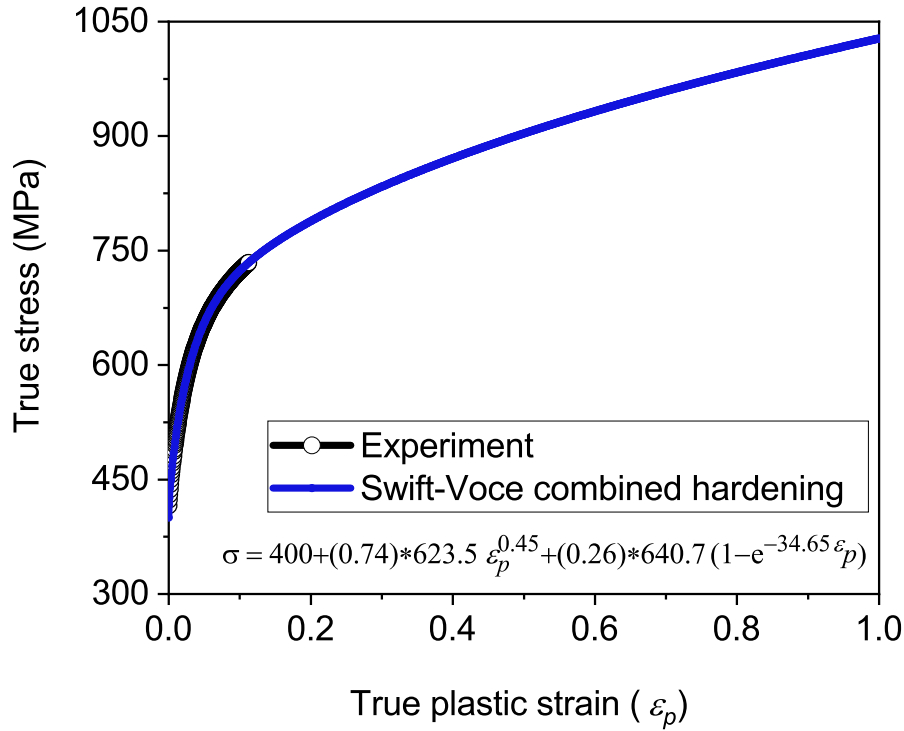


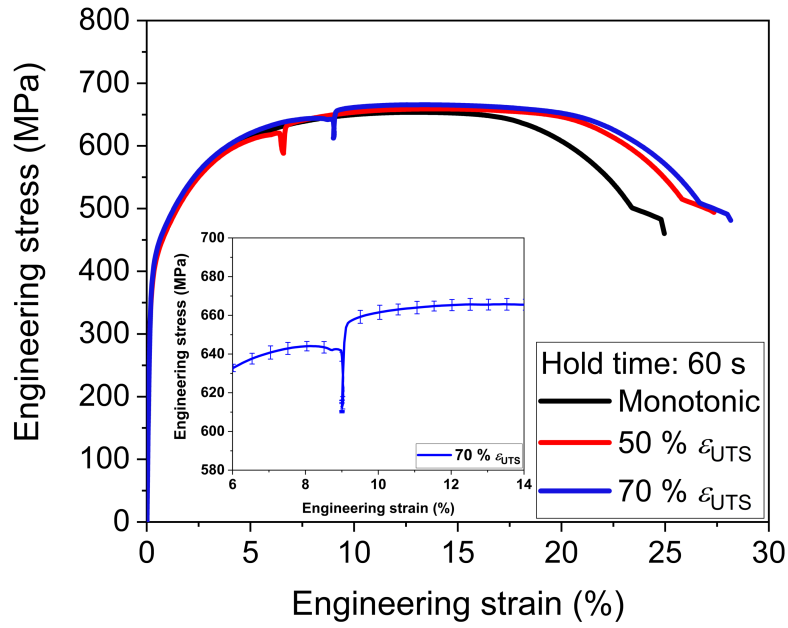
Figure 3: True tensile stress-strain curve for a uniaxial specimen tested at a strain rate of  $0.042 \text{ s}^{-1}$  and fitted with the combined Swift-Voce hardening law for DP600 steel.

### 153 3. Results and discussion

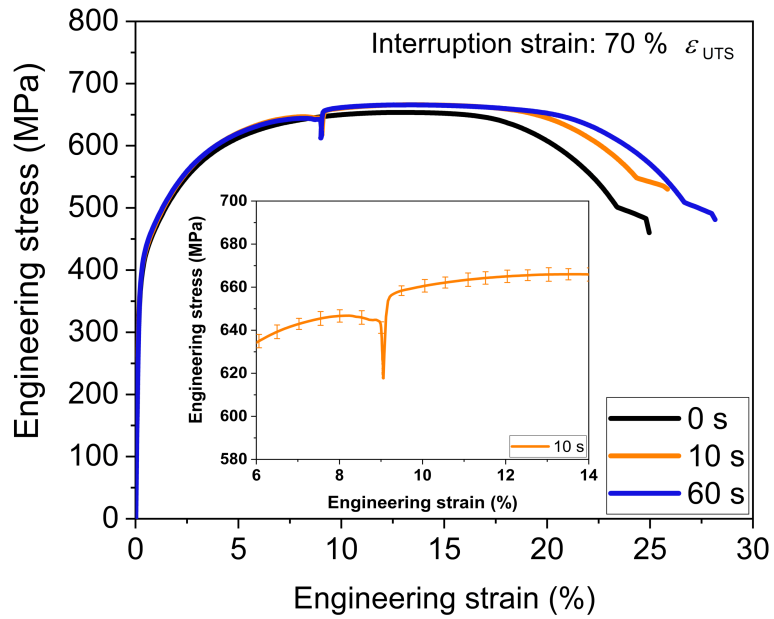
154 The microstructure of the base metal is characterized. The characterization procedure  
 155 and results can be referred to in Appendix B and C.

#### 156 3.1. Ductility improvement: Uniaxial tensile test

157 The stress-strain response of the material subjected to monotonic and stress relaxation  
 158 loading is shown in Figure.4. A strain rate of,  $\dot{\epsilon} = 0.042 \text{ s}^{-1}$  was used to conduct  
 159 monotonic and stress relaxation tests. This strain rate corresponds to the maximum  
 160 value reached at hole edges during HET, as estimated from finite element analysis (Section  
 161 2.1). Improvement in ductility was observed when the tensile specimen was subjected to  
 162 stress relaxation at different combinations of pre- strain and relaxation time. Following  
 163 earlier literature [33–35], the improvement in ductility due to uniaxial stress relaxation  
 164 is quantified using  $\epsilon_r = \frac{\epsilon_{relax}}{\epsilon_{mono}}$ , where  $\epsilon_{relax}$  and  $\epsilon_{mono}$  refers to true uniform elongations  
 165 with and without stress relaxation, respectively.



(a)



(b)

Figure 4: Engineering stress–strain curves for uniaxial tensile specimens subjected to (a) stress relaxation for 60 s hold time at different interruption strains (b) stress relaxation at 70 % of strain corresponding to that at the UTS for different hold times tested at  $0.042 \text{ s}^{-1}$ . (Average values of stress-strain curves are reported, standard deviations for stress strain curves are shown only for few cases for clarity.)

166 Figure.5(a) and (b) shows the effects of pre-strain and relaxation time on ductility  
 167 improvement, respectively. The ductility improvement ( $\epsilon_r$ ) increases with pre-strain and

168 relaxation hold time, which are similar to the findings reported in the literature [33–35,  
 169 39]. The summary of ductility improvement due to stress relaxation are tabulated in 5

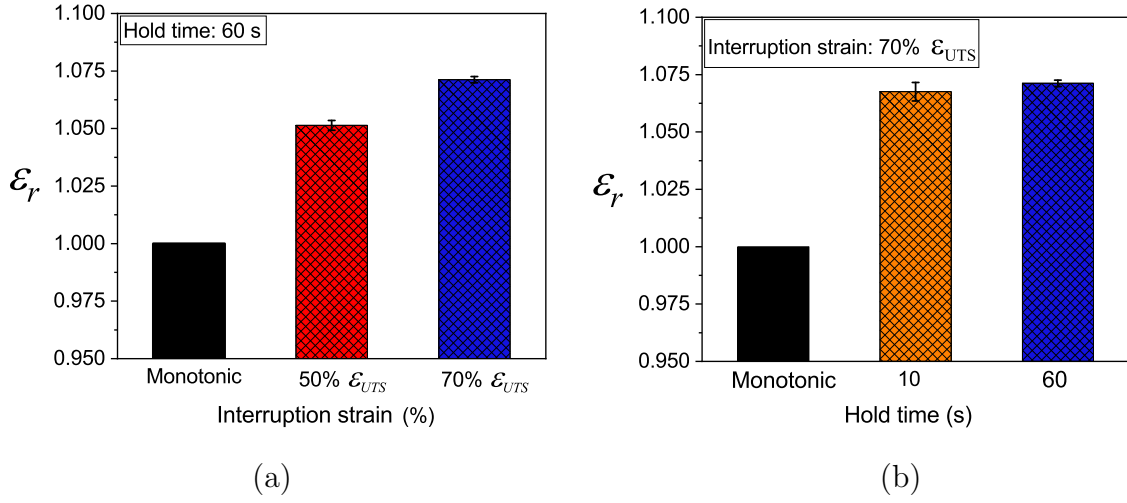


Figure 5: Ductility improvement due to uniaxial stress relaxation test (a) effect of pre-strain (b) effect of hold time.

Table 5: Improvement in ductility due to uniaxial stress relaxation.

Interruption strain (% UTS)	Time (s)	Ductility improvement (%)
50	10	5.13 ± 0.002
70	10	6.75 ± 0.004
70	60	7.12 ± 0.001

170 As reported in our earlier work [34, 35], the  $\epsilon_r$  is empirically fit using regression  
 171 analysis.  $\epsilon_r = f(\epsilon, \dot{\epsilon}, t)$ ; ( $\epsilon$ ,  $\dot{\epsilon}$  and  $t$  are true strain, true strain rate, and time,  
 172 respectively).  $\dot{\epsilon}$  and  $t$  are coupled to non-dimensionalize the variables of the regression  
 173 equation. The empirical relation obtained for DP600 steel is expressed as (eq.4). The  
 174 coefficient of determination,  $R^2$ , of the fit is 0.95.

$$\epsilon_r = 1.22 \times \left\{ \epsilon^{0.055} \times (\dot{\epsilon} \times t)^{0.0019} \right\} \quad (4)$$

### 175 3.2. Hole expansion test

176 HET were carried out as explained in Section 2.3. Holes were prepared both by drilling  
 177 and boring. Material separation during machining processes such as drilling and boring

178 induce micro-cracks on the surface that serve as crack initiation sites during HET. During  
179 the later stages of HET, through-thickness cracks developed and samples failed without  
180 localized necking. Microstructural investigation near the hole edge (Figure.6) reveals that  
181 crack propagated along the ferrite-martensite interface. Ferrite being a softer and more  
182 ductile phase compared to martensite, sustains large plastic deformation compared to  
183 martensite. This inhomogeneity in plastic deformation behavior of constituent phases  
184 initiates voids at the inter-phase boundaries [40–42] and possibly results in decohesion  
185 in the inter-phase region. Therefore, failure of the material at the hole edge plays a  
186 dominant role during HET.

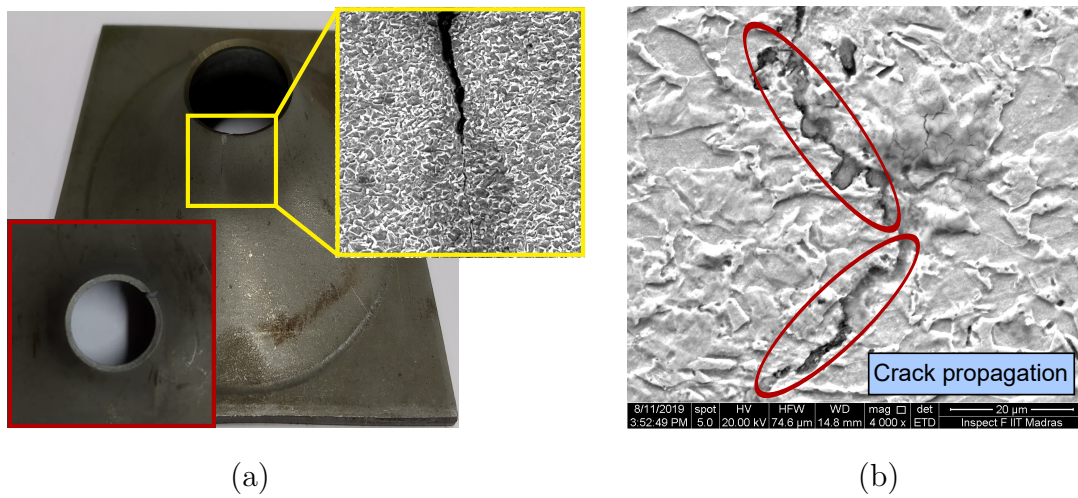


Figure 6: (a) Deformed HET sample showing the investigated region along with microstructural evidence, (b) Enlarged figure showing the crack propagation along the ferrite-martensite interface.

187 Figure.7 shows HER (Eq.1) and equivalent failure strain (Eq.2) in drilled and bored  
188 edges. It is observed that bored edge samples failed at higher equivalent failure strain and  
189 thus showed higher HER. This suggests that HER and equivalent failure strain value is  
190 sensitive to the initial hole preparation technique, in agreement with previously reported  
191 results [3, 9, 43, 44].

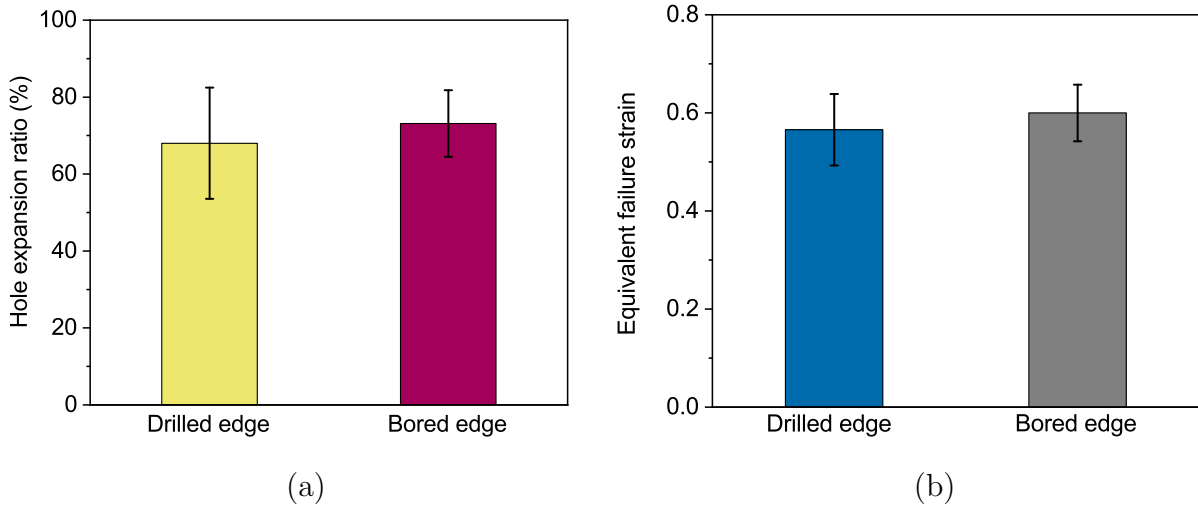


Figure 7: Comparison of monotonic (a) Hole expansion ratios of the DP600 steel (b) Equivalent failure strain obtained during the hole expansion tests for the drilled and bored edges (Monotonic HET - samples tested without punch interruption).

192 The observed difference in HER due to hole edge quality can be correlated with surface  
 193 roughness (Figure.8). The measured average surface roughness ( $R_a$ ) of a drilled hole edge  
 194 is  $4.32 \pm 0.192 \mu m$  and that of a bored edge is  $2.32 \pm 0.145 \mu m$ . The surface roughness  
 195 of drilled edges is nearly twice that of the bored edge. As explained earlier, micro-cracks  
 196 developed during the drilling process. The boring process is a finishing process, post  
 197 drilling and hence the micro-cracks formed are relatively less than those at drilled edges.  
 198 Since the machining parameters of both drilling and boring can influence the surface  
 199 roughness, it is prudent to correlate the influence of hole edge using surface roughness  
 200 rather than the manufacturing process. While such an attempt is of interest, the present  
 201 work focuses on the time-dependent mechanical behavior on the HER improvement.

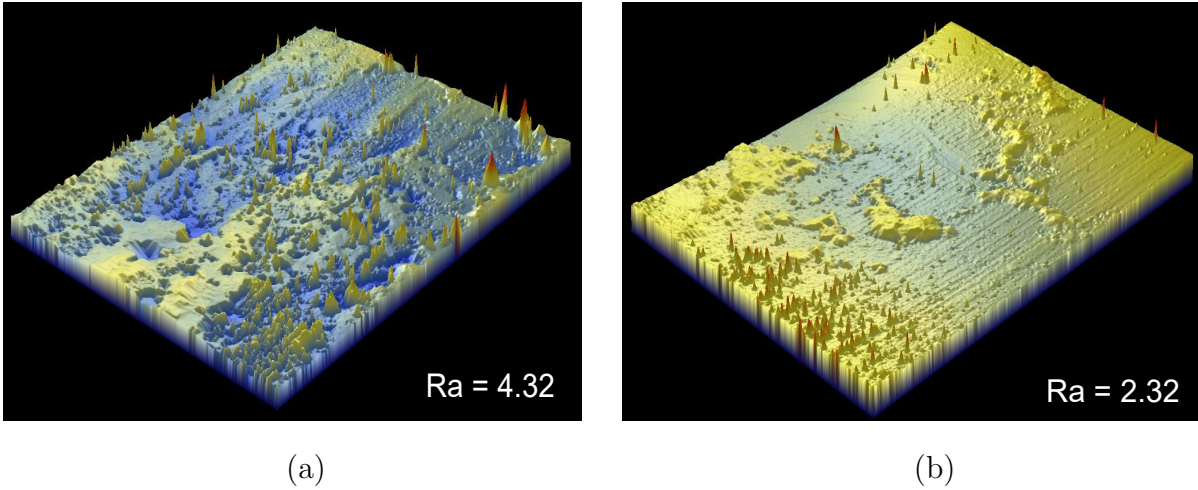
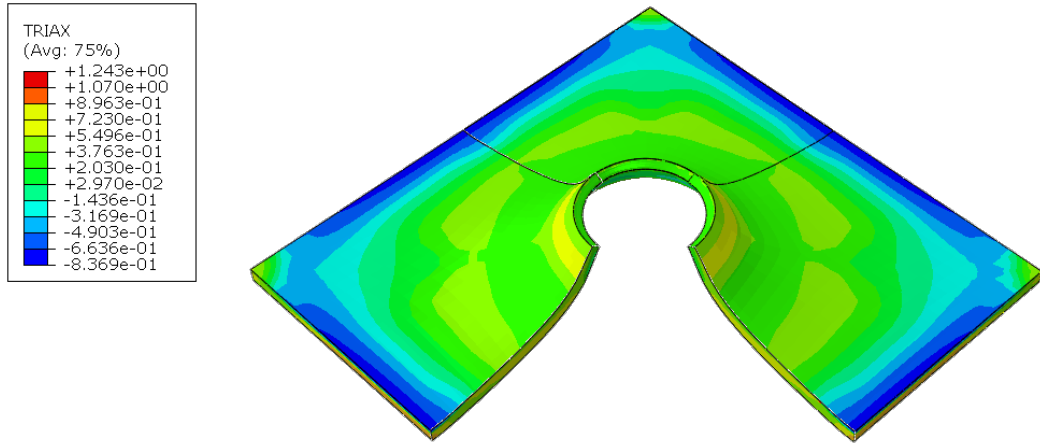


Figure 8: Surface topography images of samples prepared using (a) Drilling (b) Boring.

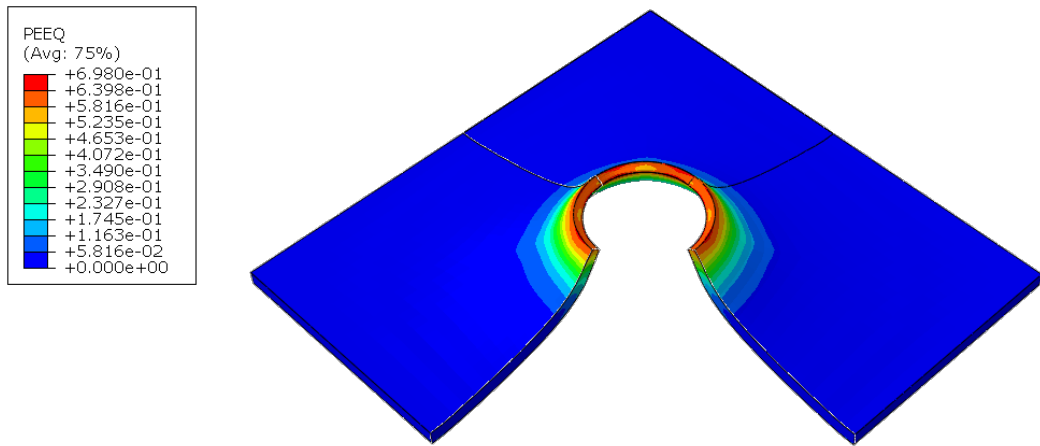
202 In addition to the edge surface, the stretch flangeability and therefore the HER can  
 203 be improved by utilizing the mechanical viscoplastic behavior or rate effect of materials,  
 204 as demonstrated in the application of a servo press [45]. Such time-dependent effects can  
 205 be studied by interrupting the HET (refer to section.3.4) without unloading.

### 206 3.3. Finite element simulation of HET

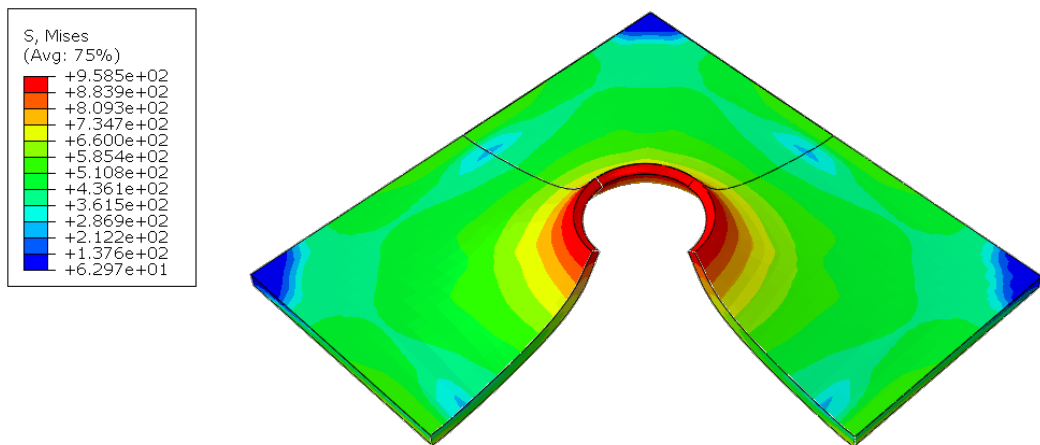
207 One problem with the traditional evaluation of HER from a HET is the possibility  
 208 of having non-uniform strains around the edges, which varies from that calculated with  
 209 the analytical expression (equation 1) based on uniform change in diameter of the hole.  
 210 Therefore, finite element modeling is routinely conducted to understand the overall  
 211 deformation behavior and stress evolution during HET. Stress triaxiality values near  
 212 the hole edge (shown in Figure.9.(a)) are in the range of (0.33 to 0.37), which is very  
 213 close to the corresponding uniaxial stress state value (0.33). From the distribution of  
 214 equivalent plastic strain and von Mises stress, Figure. 9.(b) and (c), it is concluded that  
 215 deformation is primarily concentrated near the hole edge and a significant amount of  
 216 stress concentration exists near the edge.



(a)



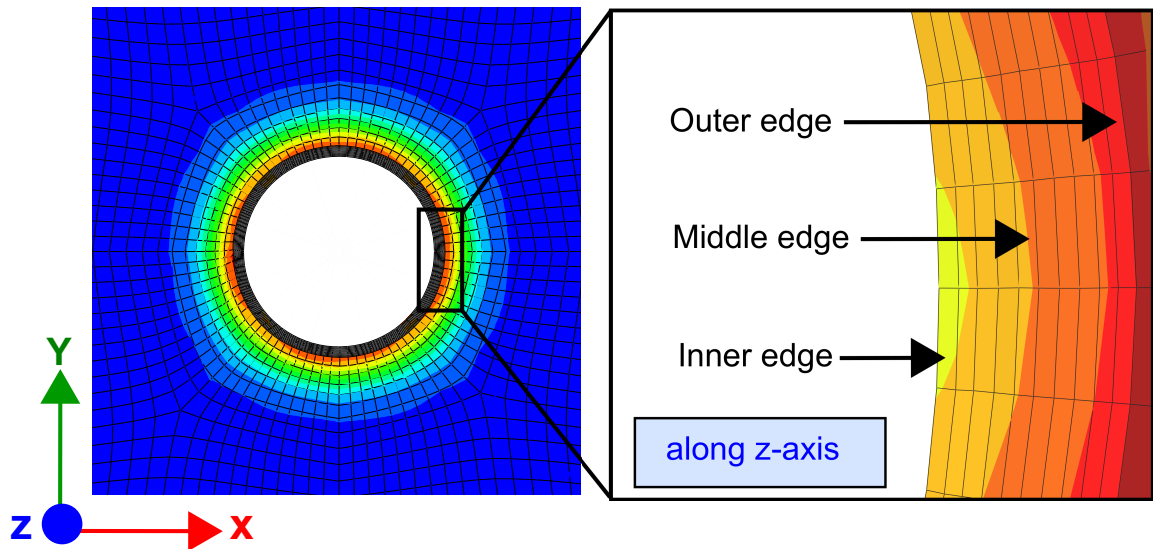
(b)



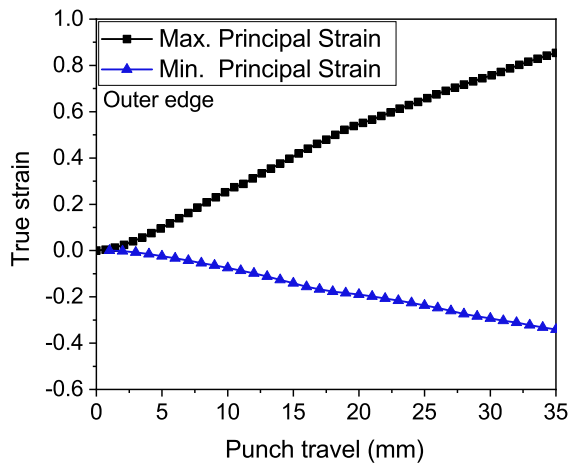
(c)

Figure 9: Finite element simulation of hole expansion: distribution of (a) Stress triaxiality (b) Equivalent plastic strain (c) von Mises equivalent stress at the time of failure ( $HER = 72.36$ ) for a drilled edge.

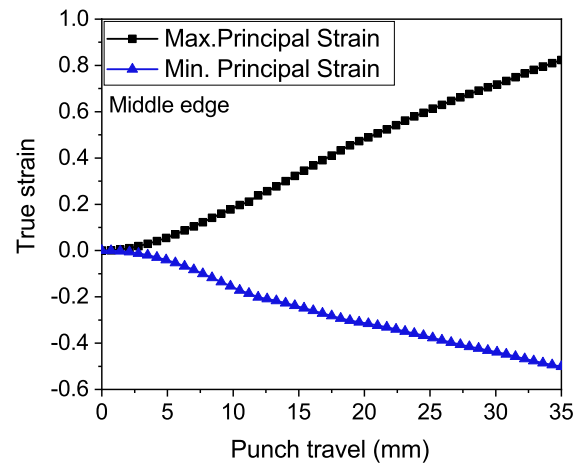
217 In order to evaluate the stress state of the hole edge, three elements (outer, middle and  
218 inner) were chosen along the through-thickness direction, as shown in Figure.10(a). The  
219 evolution of maximum and minimum principal strain with punch travel at outer, middle  
220 and inner edges is shown in Figure.10(b),(c) and (d), respectively. For isotropic materials,  
221 the strain path corresponding to the uniaxial state of stress is given by ( $\epsilon_1 = -2\epsilon_2$ ).  
222 The estimated major and minor principal strains plotted in Figure.10(e) indicates that  
223 the outer and middle portions of the edge follow a uniaxial strain path. The inner  
224 edge, however deviates from the uniaxial strain path possibly due to varying compressive  
225 stresses and friction conditions between the sheet and the conical punch.



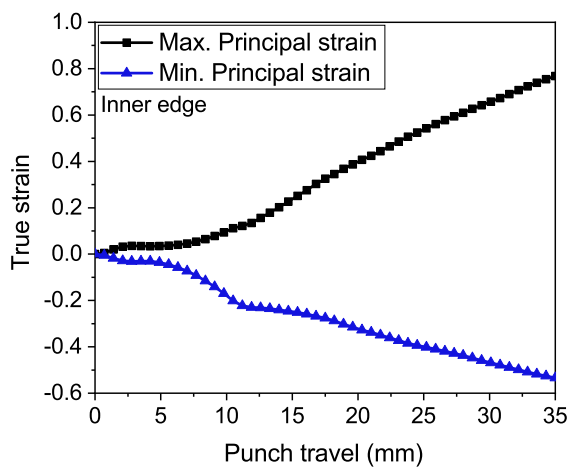
(a)



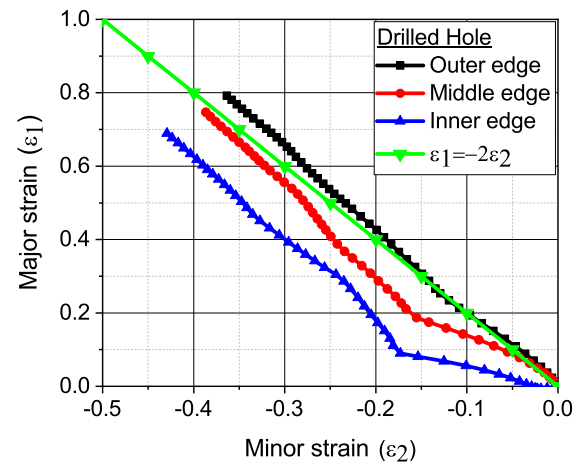
(b)



(c)



(d)



(e)

Figure 10: (a) Deformed mesh after hole expansion test simulation. Evolution of principal strain history estimated at (b) Outer, (c) Middle and (d) Inner edge positions as a function of punch travel. (e) Strain path evolution during hole expansion test simulation suggesting uniaxial tension behavior prevails at the hole edge.

226 The experiments and FE results show that the HET is controlled by the hole edge  
 227 state and the edge is predominantly under a uniaxial stress state. Thus, it is reasonable  
 228 to relate the deformation behavior during a typical interrupted HET and uniaxial stress  
 229 relaxation test. Any deviation between the trend of HET and uniaxial tension could  
 230 therefore be attributed to the friction effect during stress relaxation. The strain rate  
 231 experienced by material at the hole edge is estimated not to exceed  $0.042 \text{ s}^{-1}$  as shown  
 232 in Figure.11.

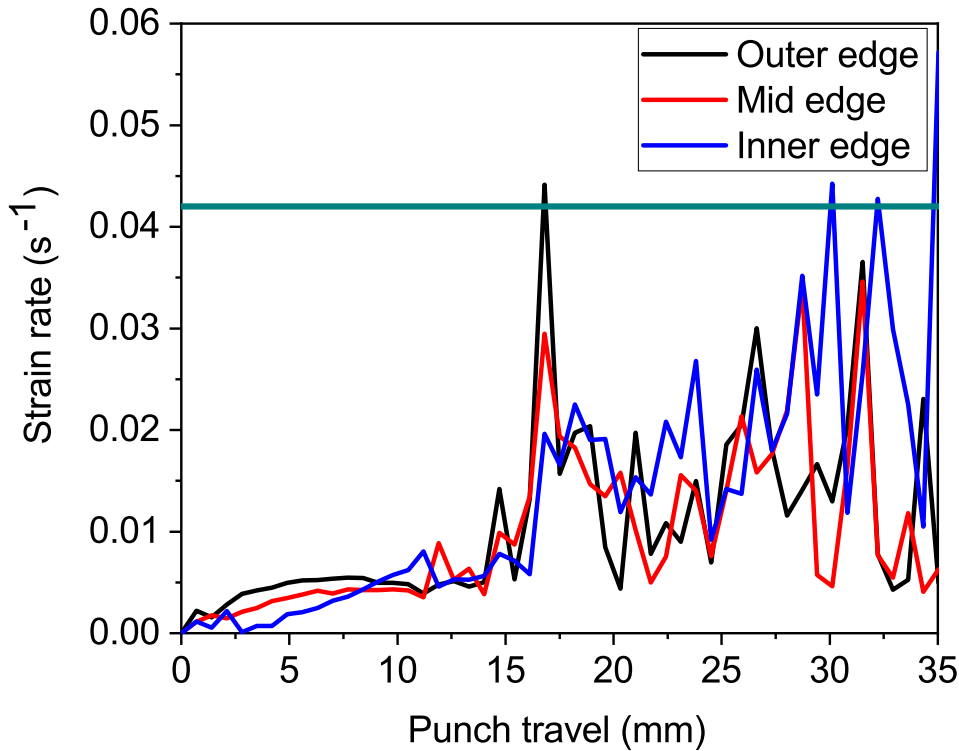


Figure 11: Strain rate evolution estimated using finite element simulation at the hole edge when deformed using a conical punch with a constant punch velocity of 10 mm/min.

### 233 3.4. Interrupted HET

234 As schematically illustrated in Figure.2, interrupted HET was performed to simulate  
 235 the effect of a servo press. Samples subjected to interrupted testing underwent  
 236 larger failure strain compared to monotonic loading, thereby resulting in higher HER  
 237 values. Figure.12 shows the sample before and after conducting HET in monotonic and  
 238 interrupted modes.

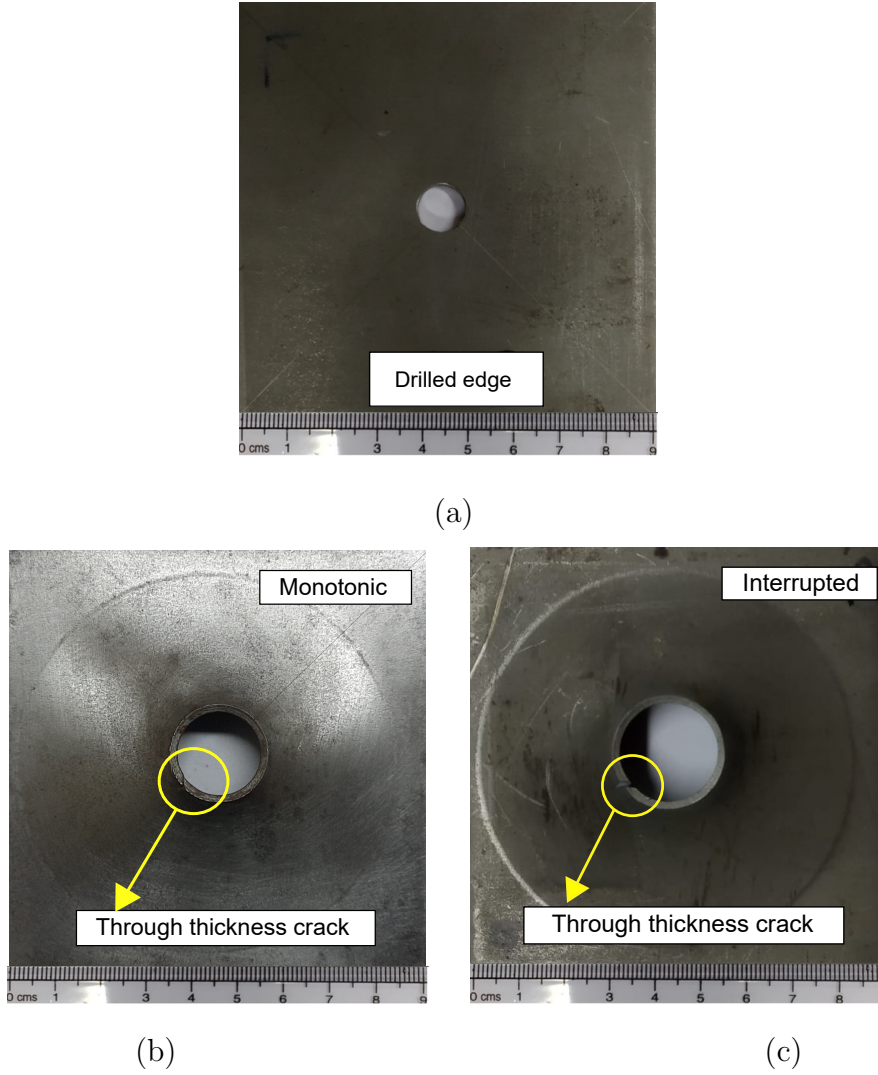
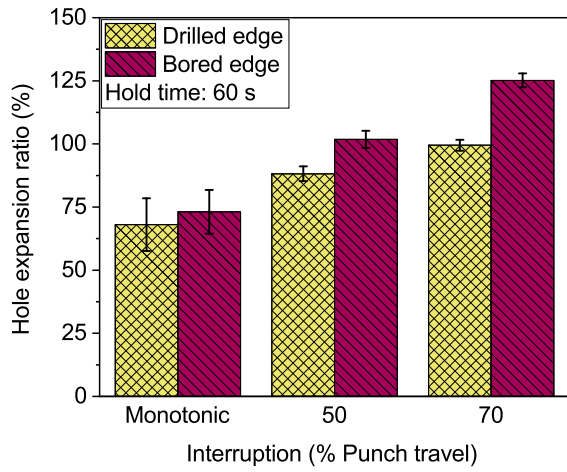


Figure 12: (a) Initial un-deformed specimen (b) Monotonically deformed specimen, (c) Specimen deformed in interrupted loading at 50 % punch travel for 60 s.

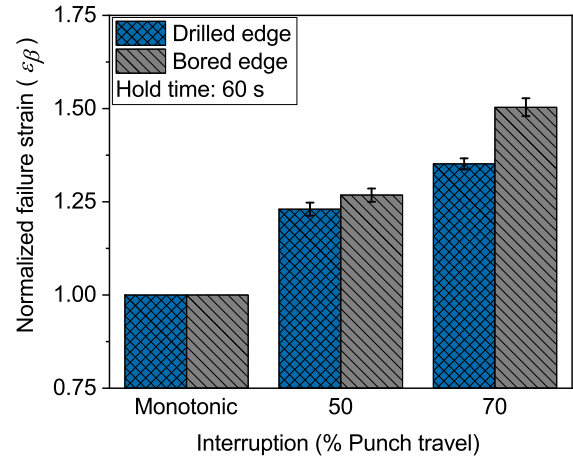
239 As the punch motion was interrupted during HET, the material was subjected to  
 240 stress relaxation which contributes to improved ductility [33–35, 39]. In addition to that,  
 241 the elastic recovery during relaxation alters the contact stresses and possibly the contact  
 242 area too. The above phenomenon, along with pressure dependent friction force at large  
 243 plastic strain, influences the mechanical behavior of HET [46–48]. The net effect in HER  
 244 is quantified using  $\epsilon_{\beta} = \frac{\epsilon_{eq}^I}{\epsilon_{eq}^M}$  where,  $\epsilon_{eq}^I$  and  $\epsilon_{eq}^M$  refers to equivalent plastic strain (eq.2) at  
 245 fracture in interrupted and monotonic loading, respectively. Under frictionless conditions,  
 246  $\epsilon_{eq}^I$  is expected to follow the trend of uniaxial stress<sup>3</sup> relaxation. It is contended that the

<sup>3</sup>The stress state near the edges in HET is near uniaxial as subsequently discussed in section.3.3

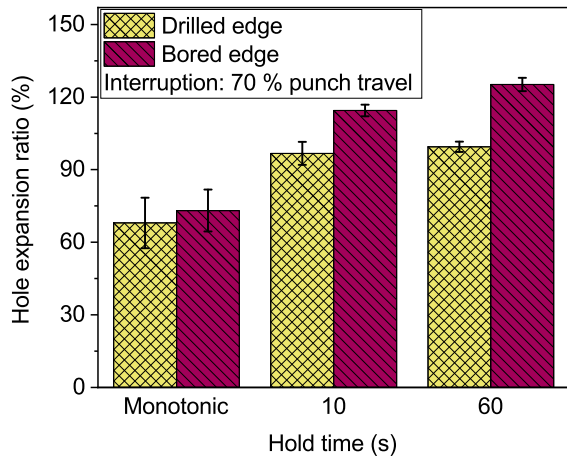
247 contact stresses due to friction alter the material behavior during relaxation. Therefore,  
248 it is pertinent to understand the interplay of material and friction effects. The material  
249 effect on ductility improvement due to stress relaxation has been reported earlier and is  
250 sensitive to relaxation time, pre-strain and strain rate [33, 34]. Accordingly, the failure  
251 strain in interrupted HET is expected to vary with hold time, punch depth and punch  
252 velocity. In an attempt to separate the friction effect, uniaxial stress relaxation tests were  
253 performed. The difference in the trend of ductility improvement in uniaxial tests ( $\epsilon_r$ ) and  
254 in HET ( $\epsilon_\beta$ ) could provide more insights on the role of friction in HER improvement during  
255 interrupted tests. In the present work, the punch velocity, which correlates with strain  
256 rate, was kept constant. The hold time and the punch depth (corresponding to pre-strain)  
257 were varied during HET, the results of which are shown in Figure.13 and tabulated in  
258 Table 6. In general, HER improvement is greater with longer hold time and higher punch  
259 depth, which is in agreement with the results seen during uniaxial stress relaxation tests.  
260 The trend of improvement is similar in both edge conditions (i.e., drilled and bored edges)  
261 during interrupted testing, however the bored edge showed larger improvement in HER.



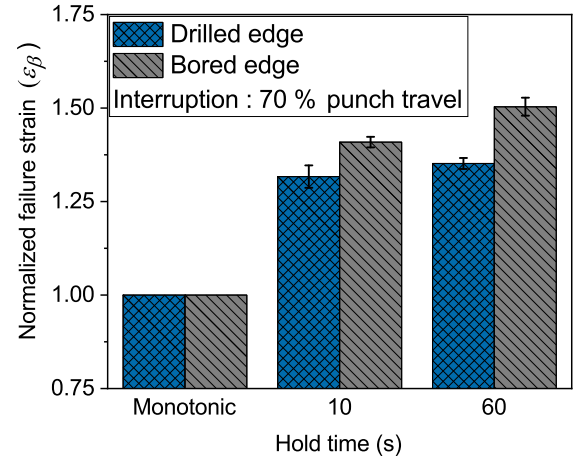
(a)



(b)



(c)



(d)

Figure 13: (a) Improvement in HER, when tests were interrupted for 60 s at 50 % and 70 % of punch travel (b) Improvement in normalized failure strain (eq.2), when tests were interrupted for 60 s at 50 % and 70 % of punch travel (c) Improvement in HER, when tests were interrupted at 70 % of punch travel for 10 s and 60 s (d) Improvement in normalized failure strain, when test is interrupted at 70 % of punch travel for 10 s and 60 s.

Table 6: Estimated HER and equivalent failure strain values in monotonic and interrupted test modes.

Test Mode	Interruption (% Punch travel)	Hold Time (s)	Edge Condition	HER	Equivalent failure strain
Monotonic	-	-	Drilled	$68 \pm 14.43$	$0.56 \pm 0.07$
	-	-	Bored	$73.12 \pm 8.66$	$0.59 \pm 0.05$
Interrupted	50	60	Drilled	$88.18 \pm 2.93$	$0.69 \pm 0.01$
			Bored	$101.83 \pm 3.40$	$0.76 \pm 0.01$
Interrupted	70	10	Drilled	$96.74 \pm 4.71$	$0.74 \pm 0.02$
			Bored	$114.46 \pm 2.42$	$0.84 \pm 0.01$
Interrupted	70	60	Drilled	$99.48 \pm 2.14$	$0.76 \pm 0.01$
			Bored	$125.17 \pm 2.74$	$0.90 \pm 0.02$

262 One of the important advantages of choosing HET to study stress relaxation effects is  
 263 the existence of a uniaxial stress state in the proximity of the hole edge where large  
 264 deformation takes place. Unlike other tests such as deep drawing, HET avoids the  
 265 complications in understanding the deformation behavior due to strain path effect and  
 266 multi-axial stress state. Therefore, as mentioned earlier, in the special condition of a  
 267 frictionless test, the HET improvement is expected to follow that obtained in uniaxial  
 268 tensile test. Experimental verification of uniaxial stress state is difficult; numerical  
 269 analysis performed in the present work is used to verify the stress state and the related  
 270 mechanics of interrupted HET test.

### 271 3.5. Contribution of friction effect in HET

272 The overall HET improvement using interrupted loading is due to stress relaxation  
 273 and friction effects. As indicated earlier, it is of interest to decouple these effects for  
 274 efficient process design in use of a servo press. Since the uniaxial tensile test is free from  
 275 friction effects, the difference between  $\epsilon_r$  and  $\epsilon_\beta$  can directly quantify the contribution  
 276 of friction in formability improvement in HET. The ductility improvement is sensitive to  
 277 the pre-strain at which relaxation is performed. The pre-strain in uniaxial tensile test is  
 278 much less compared to HET due to necking failure in the former. Since uniaxial state of  
 279 stress exist near the hole edge therefore  $\epsilon_r$  corresponding to equivalent strain during HET  
 280 is calculated by extrapolating eq.4 as a first approximation.  $\epsilon_\beta$  and  $\epsilon_r$  (corresponding to  
 281 frictionless condition) for different combinations of interruption strain and hold time are

282 compared in Figure 14. and tabulated in Table 7.

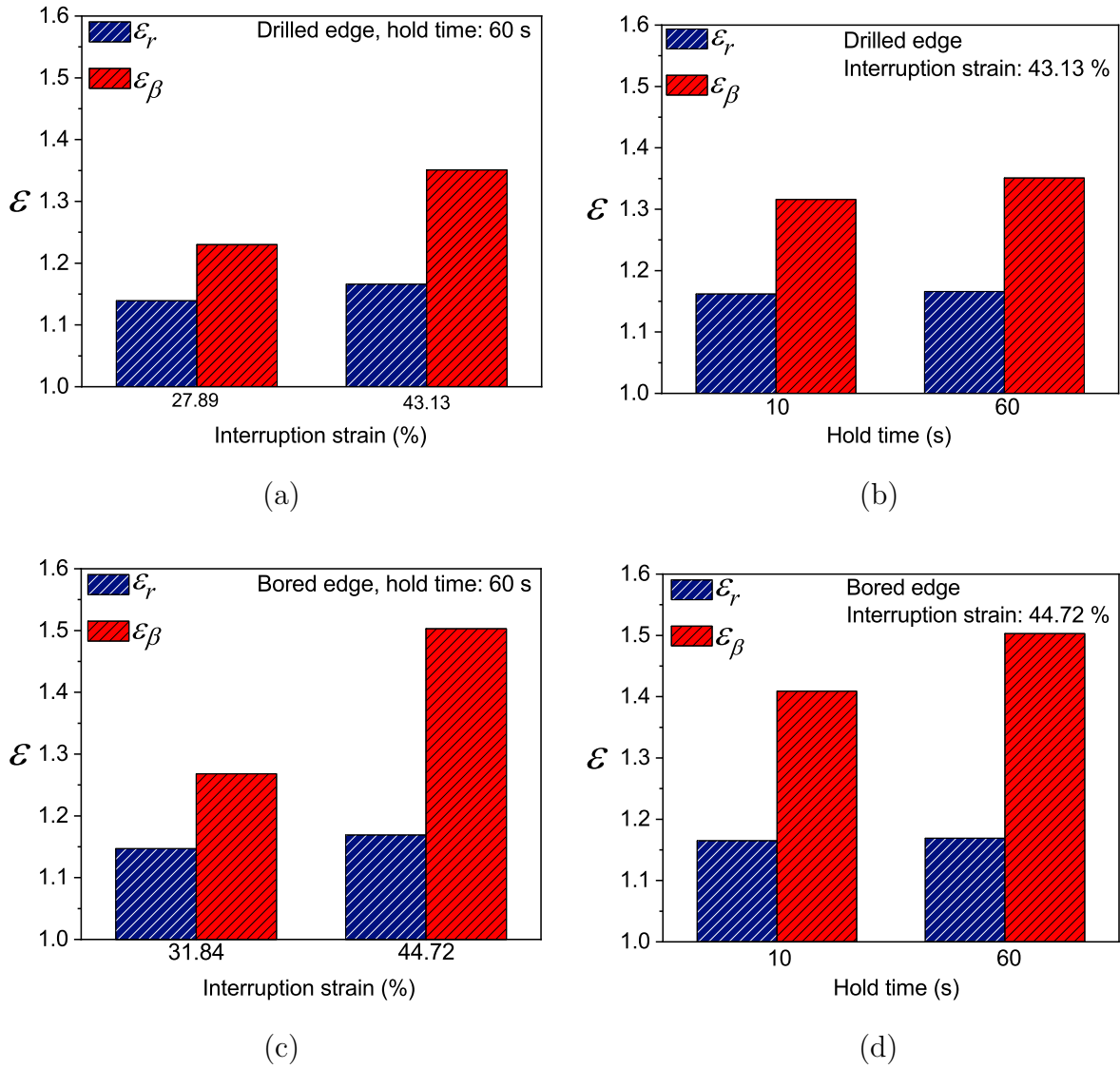


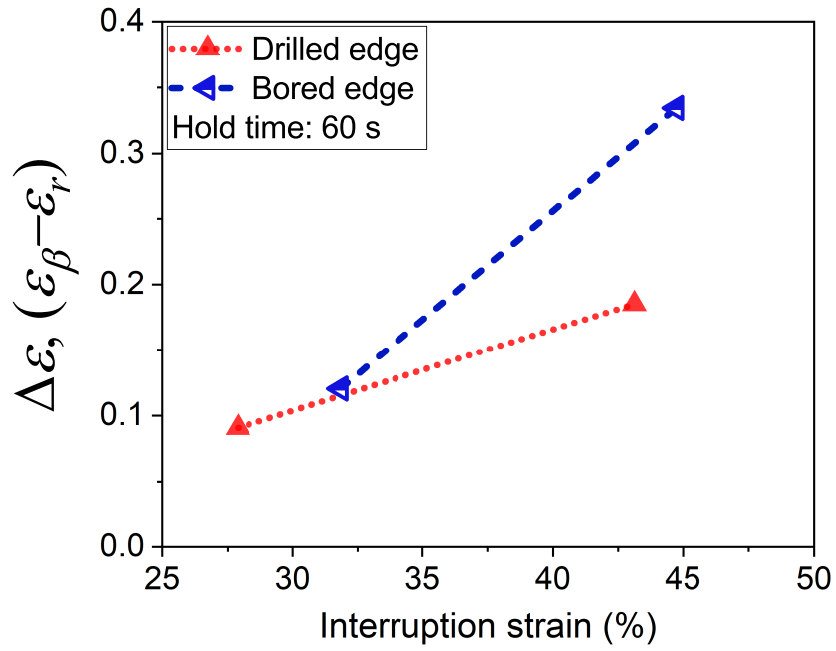
Figure 14: Comparing uniaxial ductility improvement in frictionless conditions on deformation ( $\epsilon_r$ ) and HER improvement ( $\epsilon_\beta$ ) due to interrupted testing in DP600 steel (a) Effect of prestrain for drilled edge, (b) Effect of hold time for drilled edge, (c) Effect of prestrain for bored edge, (d) Effect of hold time for bored edge.

Table 7: Comparison of strain ratio in uniaxial tensile test and HET.

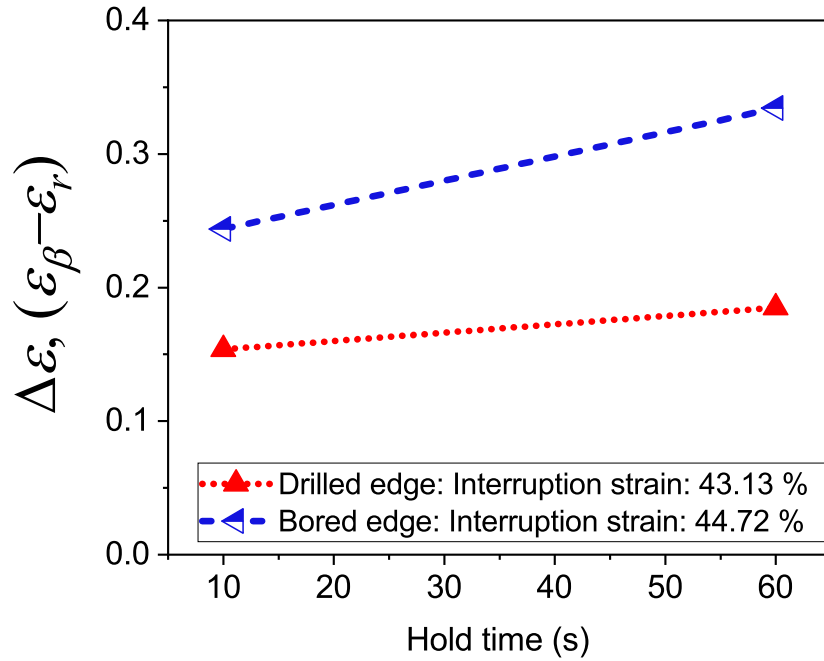
Experiment		Hold time (s)	Equivalent interruption strain (%)	$\epsilon_r$	$\epsilon_\beta$	$\Delta\epsilon = \epsilon_\beta - \epsilon_r$
Uniaxial tensile test		60	6.32	1.051	-	-
		10	8.98	1.067	-	-
		60	8.98	1.071	-	-
HET	Drilled edge	60	27.89	1.139	1.230	0.091
		10	43.13	1.162	1.316	0.154
		60	43.13	1.166	1.351	0.185
	Bored edge	60	31.84	1.147	1.268	0.121
		10	44.72	1.165	1.409	0.244
		60	44.72	1.169	1.503	0.334

283 It is seen that in general,  $\epsilon_\beta > \epsilon_r$  in all cases (Table 7) indicating definite and positive  
284 influence of friction in the formability improvement when using a servo press. Where,  $\epsilon_r$   
285 and  $\Delta\epsilon = (\epsilon_\beta - \epsilon_r)$  provides the contributions of stress relaxation and friction, respectively,  
286 in time-dependent formability improvement as reported in servo press applications.

287  $\Delta\epsilon$  was found to be sensitive to both pre-strain and holding time, although the latter's  
288 influence was negligible as shown in Figure.15. For instance, in the case of the drilled  
289 edge,  $\Delta\epsilon$  varied from 0.091 to 0.185 on increasing the pre-strain from 27.89 to 43.13;  
290 whereas, for the bored edge,  $\Delta\epsilon$  varied from 0.121 to 0.334 on increasing the pre-strain  
291 from 31.84 to 44.72 This suggests that the formability improvement due to the friction  
292 effect is increased when the interruption is performed at higher pre-strain (and therefore  
293 higher stress). On increasing the hold time from 10 s to 60 s only minimal increment in  $\Delta\epsilon$   
294 is observed for both the drilled and bored edge suggesting that formability improvement  
295 due to the friction effect is mostly independent of hold time.



(a)



(b)

Figure 15: Comparing the friction effect in drilled and bored edge  $\Delta\epsilon = (\epsilon_\beta - \epsilon_r)$  due to interrupted HET (a) Effect of pre-strain (b) Effect of hold time.

296 These observations indicate that the friction effect is primarily due to elastic recovery  
 297 and pressure-dependent friction coefficient, both of which are relatively time-independent.  
 298 The stress drop during interrupted HET reduces the mean stress in the contact region.

299 Since the friction coefficient during deformation is pressure-dependent [49–51], the  
300 reduced friction coefficient contributes positively to the formability improvement. In  
301 addition to that, the elastic recovery during interruption locally changes the contact area  
302 [46], which reduces the thinning rate of the sheet and results in higher HER. However,  
303 separating the contribution of friction coefficient and elastic recovery needs additional  
304 experiments and is planned for future work.

305 It is of interest to note that  $\Delta\epsilon$  under similar equivalent strain is different for the drilled  
306 and bored edges. The role of stress relaxation on the damage process is beyond the scope  
307 of present work, the above result provides future scope for developing time-dependent  
308 evolution of variables in a continuum damage model.

#### 309 4. Conclusions

310 The present study reports the effect of interrupted loading on stretch-flangeability in  
311 DP600 steel. The effect is evaluated for two different edge qualities manufactured by  
312 drilling and boring. Following are the important conclusions which can be drawn from  
313 the present work.

- 314 1. Compared to monotonic HET, interrupted loading significantly increased the HER.  
315 It is shown that the effect of pre-strain plays a larger role compared to hold time  
316 during interrupted testing.
- 317 2. The influence of edge quality suggests that the damage process controlling fracture  
318 behavior is also influenced by interrupted tests.
- 319 3. The overall enhanced HER was due to the two concurrent effects, stress relaxation  
320 and friction. The contribution of stress relaxation is estimated by extrapolating an  
321 empirical equation for ductility improvement obtained from uniaxial tensile tests  
322 under similar conditions.
- 323 4. The HER improvement in the present study (including drilled and bored edges),  
324  $\epsilon_\beta$ , varied between 23 % to 50.3 %, of which the contribution of stress relaxation  
325 was within a narrow range of 13.9 % to 16.9 %.
- 326 5. The friction effect contributed around 9 % to 33.4 % to HER improvement. The  
327 friction effect is strongly dependent on the pre-strain and to a lesser extent on the

328 hold time. Edge quality strongly influences the contribution from the friction effect  
 329  $(\epsilon_\beta - \epsilon_r)$ , whereas that due to stress relaxation is relatively constant. The results  
 330 indicate the transient effect on the damage evolution process controls fracture  
 331 behavior in HET.

## 332 5. Acknowledgement

333 Authors would like to acknowledge ArcelorMittal for supplying the steel used in this  
 334 work. Authors would also like to acknowledge DST–FIST, for funding the Scanning  
 335 Electron High Resolution Microscope (FESEM) joint facility, Dept. of Mechanical  
 336 Engineering and Dept. of Physics, IIT Madras. Authors would like to acknowledge Mr.  
 337 Abrar Salam, Research scholar, and Mr. Sundar Kumar, Apprentice, Metal Forming  
 338 Laboratory, Department of Metallurgical and Materials Engineering, IIT Madras for  
 339 helping in conducting hole expansion tests. One of the authors, Kali Prasad, would  
 340 like to acknowledge the help from Mr. Sahil Bharti (a Ph.D. scholar in the Mechanical  
 341 Engineering Department, IIT Madras) for fruitful discussion regarding simulation work.

## 342 Appendix A. Finite element simulation

343 The Lankford coefficients were calculated from experiments and are tabulated in Table  
 344 A.8. The HET simulations were performed assuming Hill48 anisotropic yield criterion  
 345 and compared with the results predicted using von Mises yield criterion. The maximum  
 346 strain in the outer edge which correlates with the onset of surface crack is predicted using  
 347 both the criteria and compared in Fig.A.16. It is observed that the effect of mechanical  
 348 anisotropy on the strain distribution is negligible.

Table A.8: Coefficients of lankford parameters

$r_0$	$r_{45}$	$r_{90}$	$\bar{r}$
0.742	1.01	0.782	0.866

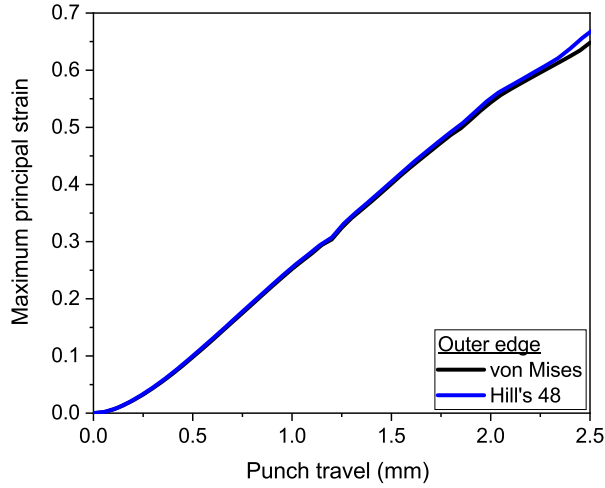


Figure A.16: Comparison of maximum principal strain with punch travel at outer edge using Hill 48 and Von Mises criteria

## 349 Appendix B. Initial Material Characterization

350 The as received DP600 samples were polished for metallographic study as per  
 351 standard polishing techniques and then etched with 2 % nital reagent for 10 s to  
 352 obtain the as received microstructure. Scanning electron microscope (SEM) (Inspect  
 353 F50 from FEI) was used to obtain the microstructure of the as received DP600 steel.  
 354 For transmission electron microscopy (TEM) investigation, the as received samples  
 355 were initially mechanically polished to 80  $\mu\text{m}$  as per standard metallographic polishing  
 356 techniques. Then 3 mm diameter discs were punched from the samples using a disc  
 357 punching machine. The samples were further thinned by using a twin jet polishing  
 358 machine to obtain an electron transparent region thereafter, TEM characterization was  
 359 performed in FEI Tecnai  $G^2$  operating at 200 kV . Initial surface roughness of the central  
 360 hole of HET specimens prepared using drilling and boring operations was characterized  
 361 using non contact optical profilometer (Wyko NT1100 Veeco Instruments, USA). Nano  
 362 indentation tests using a Berkovich diamond indenter (HYSITRON Instruments) were  
 363 performed to characterize the martensite and ferrite phases. The indentation tests were  
 364 performed on individual phases with a maximum load of 2 mN at the loading rate of  
 365 4 mN/min. Care was taken in selecting the appropriate indentation locations to avoid  
 366 grain boundary effects.

367 **Appendix C. Material Characterization Results**

368 Figure.C.17(a) & (b) show the microstructure and bright field micrograph of the  
 369 as received DP600 sheet obtained using a scanning electron microscope (SEM) and a  
 370 transmission electron microscope (TEM), respectively. The microstructure reveals the  
 371 presence of uniformly distributed martensite islands in the ferrite matrix, details of which  
 372 are tabulated in Table C.9. Average grain size of the individual phases were determined  
 373 using the line intercept method following ASTM E112-13 [52].

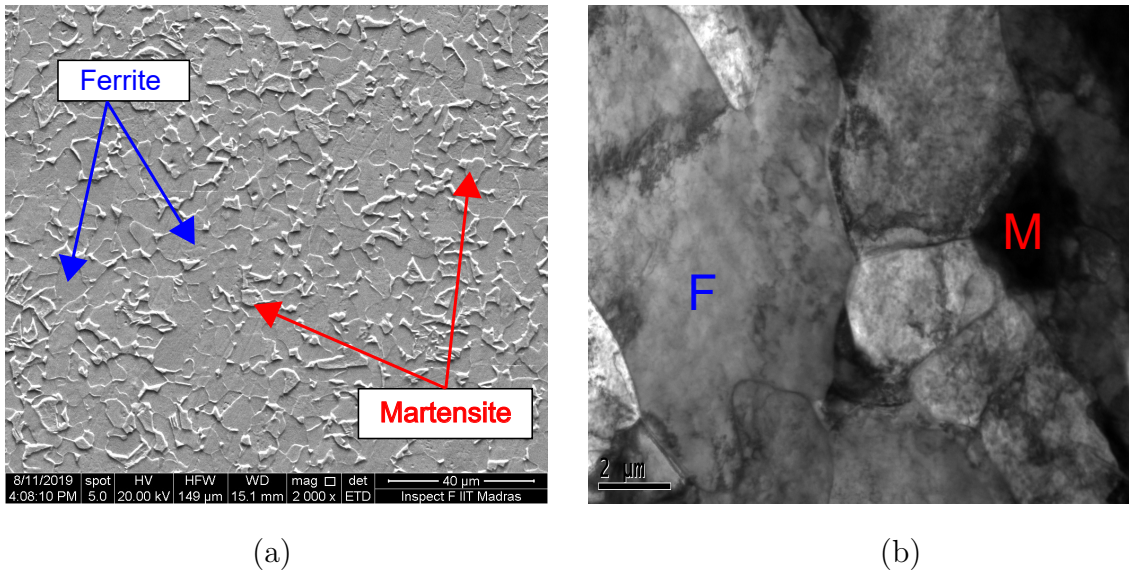


Figure C.17: (a) Microstructure of as received DP600 steel (b) Bright field micrograph showing ferrite (F) and martensite (M) phases.

Table C.9: Microstructural parameters of DP600 steel (uncertainties are given in  $\pm 1$  standard deviation).

Steel	Ferrite grain size ( $\mu m$ )	Martensite grain size ( $\mu m$ )	Martensite phase fraction (%)
DP600	$4.1 \pm 1.6$	$2.5 \pm 1.4$	$22 \pm 1$

374 The hardness of ferrite and martensite phases was measured using nano-indentation  
 375 tests. The indentation response of phases was estimated from the measured load vs  
 376 penetration depth curves as shown in Figure.C.18. It can be seen that for a given  
 377 indentation load, the average penetration depth of ferrite is higher than that of martensite,  
 378 which indicates higher indentation resistance offered by martensite (Table: C.10).

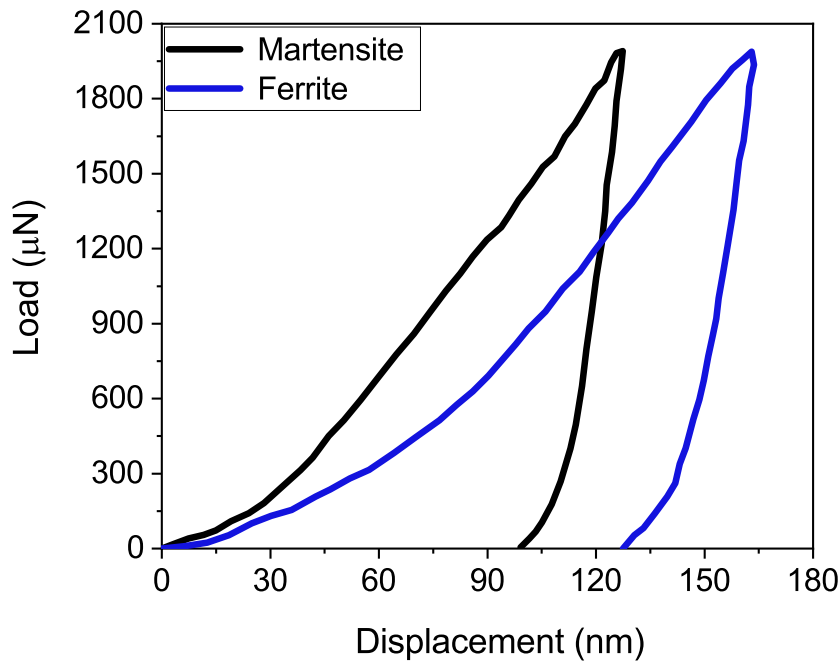


Figure C.18: Load-displacement curves of ferrite and martensite phases for the as-received DP600 steel.

Table C.10: Hardness characterization of DP600 steel.

Martensite phase $V_m$ (%)	$22 \pm 1$
Martensite Hardness $H_M$ (GPa)	$4.34 \pm 0.31$
Ferrite Hardness $H_F$ (GPa)	$3.49 \pm 0.39$

## 379 References

- 380 [1] H. Qu, G. M. Michal, A. H. Heuer, A 3rd generation advanced high-strength steel  
 381 (AHSS) produced by dual stabilization heat treatment (DSHT), Metallurgical and  
 382 Materials Transactions A 44 (10) (2013) 4450–4453. doi:10.1007/s11661-013-1871-z.
- 383 [2] J. Walker, D. J. Thomas, Y. Gao, Effects of shot peening and pre-strain on the  
 384 fatigue life of dual phase martensitic and bainitic steels, Journal of Manufacturing  
 385 Processes 26 (2017) 419 – 424. doi:https://doi.org/10.1016/j.jmapro.2017.03.010.
- 386 [3] C. Pathak, N. and Butcher, M. Worswick, Assessment of the critical parameters  
 387 influencing the edge stretchability of advanced high-strength steel sheet,  
 388 Journal of Materials Engineering and Performance 25 (11) (2016) 4919–4932.  
 389 doi:10.1007/s11665-016-2316-9.

- 390 [4] C. Tasan, J. Hoefnagels, C. ten Horn, M. Geers, Experimental analysis of strain path  
391 dependent ductile damage mechanics and forming limits, *Mechanics of Materials*  
392 41 (11) (2009) 1264 – 1276. doi:<https://doi.org/10.1016/j.mechmat.2009.08.003>.
- 393 [5] S. Chatterjee, H. K. D. H. Bhadeshia, Stretch-flangeability of strong  
394 multiphase steels, *Materials Science and Technology* 23 (5) (2007) 606–609.  
395 arXiv:<https://doi.org/10.1179/174328407X179511>, doi:10.1179/174328407X179511.
- 396 [6] Z. Cui, L. Gao, Studies on hole-flanging process using multistage incremental  
397 forming, *CIRP Journal of Manufacturing Science and Technology* 2 (2) (2010) 124  
398 – 128. doi:<https://doi.org/10.1016/j.cirpj.2010.02.001>.
- 399 [7] G. Centeno, M. Silva, V. Cristino, C. Vallellano, P. Martins, Hole-flanging by  
400 incremental sheet forming, *International Journal of Machine Tools and Manufacture*  
401 59 (2012) 46 – 54. doi:<https://doi.org/10.1016/j.ijmachtools.2012.03.007>.
- 402 [8] ISO, metallic materials – method of hole expanding test; 2009. <http://www.iso.org>  
403 [accessed may 17, 2016].
- 404 [9] L. Xu, F. Barlat, M. G. Lee, K. S. Choi, X. Sun, Hole expansion of dual  
405 phase steels, *WIT Transactions on The Built Environment* 124 (2012) 75 – 83.  
406 doi:10.2495/HPSM120071.
- 407 [10] S. K. Paul, The effect of deformation gradient on necking and failure  
408 in hole expansion test, *Manufacturing Letters* 21 (2019) 50 – 55.  
409 doi:<https://doi.org/10.1016/j.mfglet.2019.08.004>.
- 410 [11] M. Taylor, K. Choi, X. Sun, D. Matlock, C. Packard, L. Xu, F. Barlat, Correlations  
411 between nanoindentation hardness and macroscopic mechanical properties in  
412 DP980 steels, *Materials Science and Engineering: A* 597 (2014) 431 – 439.  
413 doi:<https://doi.org/10.1016/j.msea.2013.12.084>.
- 414 [12] L.Chen, J.-K. Kim, S.-K. Kim, G.-S. Kim, K.-G. Chin, B.C. De Cooman,  
415 Stretch-flangeability of high Mn TWIP steel, *steel research international* 81 (7)  
416 (2010) 552–568. doi:10.1002/srin.201000044.

- 417 [13] Correlation between fracture toughness and stretch-flangeability of  
418 advanced high strength steels, *Materials Letters* 180 (2016) 322 – 326.  
419 doi:<https://doi.org/10.1016/j.matlet.2016.05.145>.
- 420 [14] R. J. Comstock, D. K. Scherrer, R. D. Adamczyk, Hole expansion in a variety of sheet  
421 steels, *Journal of Materials Engineering and Performance* 15 (6) (2006) 675–683.  
422 doi:10.1361/105994906X150830.
- 423 [15] D. Casellas, A. Lara, D. Frómeta, D. Gutiérrez, S. Molas, L. Pérez, J. Rehr, C. Suppan,  
424 Fracture toughness to understand stretch-flangeability and edge cracking  
425 resistance in ahss, *Metallurgical and Materials Transactions A* 48 (1) (2017) 86–94.  
426 doi:10.1007/s11661-016-3815-x.
- 427 [16] S. K. Paul, Correlation between hole expansion ratio (HER)  
428 and notch tensile test, *Manufacturing Letters* 20 (2019) 1 – 4.  
429 doi:<https://doi.org/10.1016/j.mfglet.2019.02.003>.
- 430 [17] J. I. Yoon, J. Jung, H. H. Lee, G.-S. Kim, H. S. Kim, Factors governing hole  
431 expansion ratio of steel sheets with smooth sheared edge, *Metals and Materials  
432 International* 22 (6) (2016) 1009–1014. doi:10.1007/s12540-016-6346-5.
- 433 [18] S. K. Paul, A critical review on hole expansion ratio, *Materialia* 9 (2020) 100566.  
434 doi:<https://doi.org/10.1016/j.mtla.2019.100566>.
- 435 [19] S. K. Paul, Effect of punch geometry on hole expansion ratio, *Proceedings  
436 of the Institution of Mechanical Engineers, Part B: Journal of Engineering  
437 Manufacture* 234 (3) (2019) 1–6. arXiv:<https://doi.org/10.1177/0954405419863222>,  
438 doi:10.1177/0954405419863222.
- 439 [20] G. K. Mandal, K. Ashok, S. K. Das, P. Biswas, R. B. Sarkar, R. Sundara Bharathy,  
440 V. C. Srivastava, Development of stretch flangeable grade steels by inclusion  
441 engineering approach, *Journal of Materials Engineering and Performance* 27 (11)  
442 (2018) 5622–5634. doi:10.1007/s11665-018-3703-1.
- 443 [21] J. I. Yoon, H. H. Lee, J. Jung, H. S. Kim, Effect of grain size on stretch-flangeability  
444 of twinning-induced plasticity steels, *Materials Science and Engineering: A* 735  
445 (2018) 295 – 301. doi:<https://doi.org/10.1016/j.msea.2018.08.052>.

- 446 [22] M. Calcagnotto, D. Ponge, D. Raabe, Effect of grain refinement to 1 $\mu$ m on strength  
447 and toughness of dual-phase steels, *Materials Science and Engineering: A* 527 (29)  
448 (2010) 7832 – 7840. doi:<https://doi.org/10.1016/j.msea.2010.08.062>.
- 449 [23] X. Fang, Z. Fan, B. Ralph, P. Evans, R. Underhill, Effects of tempering  
450 temperature on tensile and hole expansion properties of a C–Mn steel,  
451 *Journal of Materials Processing Technology* 132 (1) (2003) 215 – 218.  
452 doi:[https://doi.org/10.1016/S0924-0136\(02\)00923-8](https://doi.org/10.1016/S0924-0136(02)00923-8).
- 453 [24] K. Hasegawa, K. Kawamura, T. Urabe, Y. Hosoya, Effects of microstructure on  
454 stretch-flange-formability of 980 mpa grade cold-rolled ultra high strength steel  
455 sheets, *ISIJ International* 44 (3) (2004) 603–609. doi:[10.2355/isijinternational.44.603](https://doi.org/10.2355/isijinternational.44.603).
- 456 [25] J. I. Yoon, J. Jung, J. G. Kim, S. S. Sohn, S. Lee, H. S. Kim, Key factors of  
457 stretch-flangeability of sheet materials, *Journal of Materials Science* 52 (13) (2017)  
458 7808–7823. doi:[10.1007/s10853-017-1012-y](https://doi.org/10.1007/s10853-017-1012-y).
- 459 [26] K. Osakada, K. Mori, T. Altan, P. Groche, Mechanical servo press  
460 technology for metal forming, *CIRP Annals* 60 (2) (2011) 651 – 672.  
461 doi:<https://doi.org/10.1016/j.cirp.2011.05.007>.
- 462 [27] T. Maeno, K. Mori, A. Hori, Application of load pulsation using servo press to plate  
463 forging of stainless steel parts, *Journal of Materials Processing Technology* 214 (7)  
464 (2014) 1379 – 1387. doi:<https://doi.org/10.1016/j.jmatprotec.2014.01.018>.
- 465 [28] K. Mori, K. Akita, Y. Abe, Springback behaviour in bending of  
466 ultra-high-strength steel sheets using CNC servo press, *International*  
467 *Journal of Machine Tools and Manufacture* 47 (2) (2007) 321 – 325.  
468 doi:<https://doi.org/10.1016/j.ijmachtools.2006.03.013>.
- 469 [29] C.-C. Kuo, H.-L. Huang, T.-C. Li, K.-L. Fang, B.-T. Lin, Optimization of the  
470 pulsating curve for servo stamping of rectangular cup, *Journal of Manufacturing*  
471 *Processes* 56 (2020) 990 – 1000. doi:<https://doi.org/10.1016/j.jmapro.2020.06.004>.
- 472 [30] P. Stemler, A. Samant, D. Hofmann, T. Altan, Impact of servo press motion on hole  
473 flanging of high strength steels, in: *WCX<sup>TM</sup> 17: SAE World Congress Experience*,  
474 SAE International, 2017. doi:<https://doi.org/10.4271/2017-01-0311>.

- 475 [31] H. Yamashita, H. Ueno, H. Nakai, T. Higaki, Technology to enhance deep-drawability  
476 by strain dispersion using stress relaxation phenomenon, in: SAE Technical Paper,  
477 SAE International, 2015. doi:10.4271/2015-01-0531.
- 478 [32] K. Hariharan, O. Majidi, C. Kim, M. Lee, F. Barlat, Stress relaxation and its effect  
479 on tensile deformation of steels, *Materials Design (1980-2015)* 52 (2013) 284 – 288.  
480 doi:https://doi.org/10.1016/j.matdes.2013.05.088.
- 481 [33] K. Hariharan, P. Dubey, J. Jain, Time dependent ductility improvement of stainless  
482 steel ss 316 using stress relaxation, *Materials Science and Engineering: A* 673 (2016)  
483 250 – 256. doi:https://doi.org/10.1016/j.msea.2016.07.074.
- 484 [34] K. Prasad, H. Krishnaswamy, J. Jain, Leveraging transient mechanical  
485 effects during stress relaxation for ductility improvement in aluminium AA  
486 8011 alloy, *Journal of Materials Processing Technology* 255 (2018) 1 – 7.  
487 doi:https://doi.org/10.1016/j.jmatprotec.2017.11.053.
- 488 [35] K. Prasad, H. Krishnaswamy, N. Arunachalam, Investigations on ductility  
489 improvement and reloading yielding during stress relaxation of dual phase  
490 Ti–6Al–4V titanium alloy, *Journal of Alloys and Compounds* 828 (2020) 154450.  
491 doi:https://doi.org/10.1016/j.jallcom.2020.154450.
- [36] Astm e8 / e8m-16a, standard test methods for tension testing of metallic  
materials, Tech. rep., ASTM International, West Conshohocken, PA (2016).  
doi:10.1520/E0008E0008M – 16A.
- [37] C. Butcher, L. Kortenaar, M. Worswick, Experimental characterization of the sheared  
493 edge formability of boron steel, IDDRG, Paris, France (2014).
- [38] S. K. Paul, S. Roy, S. Sivaprasad, H. N. Bar, S. Tarafder, Identification of post-necking  
495 tensile stress–strain behavior of steel sheet: An experimental investigation using digital  
496 image correlation technique, *Journal of Materials Engineering and Performance* 27(11)  
497 (2018) 5736–5743. doi:https://doi.org/10.1007/s11665-018-3701-3.
- [39] A. Varma, A. Gokhale, J. Jain, K. Hariharan, P. Cizek, M. Barnett, Investigation of stress  
499 relaxation mechanisms for ductility improvement in SS316L, *Philosophical Magazine*  
500 98 (3) (2018) 165–181. doi:10.1080/14786435.2017.1398422.

- [40] G.Avramic-Cingara, Ch.A.R.Saleh, M.K.Jain, D. Wilkinson, Void nucleation and  
502 growth in dual-phase steel 600 during uniaxial tensile testing, *Metallurgical and Materials*  
503 *Transactions A* 40A (2009) 3117–3127. doi:<https://doi.org/10.1007/s11661-009-0030-z>.
- [41] N. Saeidi, F. Ashrafizadeh, B. Niroumand, M. Forouzan, S. M. mofidi], F. Barlat, Void  
505 coalescence and fracture behavior of notched and un-notched tensile tested specimens in  
506 fine grain dual phase steel, *Materials Science and Engineering: A* 644 (2015) 210 – 217.  
507 doi:<https://doi.org/10.1016/j.msea.2015.07.036>.
- [42] K. Bandyopadhyay, S. Panda, P. Saha, V. Baltazar-Hernandez, Y. Zhou,  
509 Microstructures and failure analyses of dp980 laser welded blanks in formability  
510 context, *Materials Science and Engineering: A* 652 (2016) 250 – 263.  
511 doi:<https://doi.org/10.1016/j.msea.2015.11.091>.
- [43] N. Pathak, C. Butcher, M. Worswick, On simulation of edge stretchability of an 800 mpa  
513 advanced high strength steel, *Journal of Physics: Conference Series* 734 (2016) 032121.  
514 doi:[10.1088/1742-6596/734/3/032121](https://doi.org/10.1088/1742-6596/734/3/032121).
- [44] N. Pathak, C. Butcher, M. J. Worswick, E. Bellhouse, J. Gao, Damage evolution  
516 in complex-phase and dual-phase steels during edge stretching, *Materials* 4 (2017).  
517 doi:[10.3390/ma10040346](https://doi.org/10.3390/ma10040346).
- [45] M. Takamura, K. Murasawa, Y. Kusuda, Y. Suzuki, T. Hakoyama, Y. Ikeda, Y. Otake,  
519 T. Hama, S. Suzuki, Investigation on stress relaxation behavior of high-strength steel  
520 sheets based on elasto-viscoplasticity, *Journal of Physics: Conference Series* 1063 (2018)  
521 012123. doi:[10.1088/1742-6596/1063/1/012123](https://doi.org/10.1088/1742-6596/1063/1/012123).
- [46] O. Majidi, F. Barlat, M.-G. Lee, D.-J. Kim, Formability of ahss under  
523 an attach–detach forming mode, *steel research international* 86 (2) (2015)  
524 98–109. arXiv:<https://onlinelibrary.wiley.com/doi/pdf/10.1002/srin.201400001>,  
525 doi:[10.1002/srin.201400001](https://doi.org/10.1002/srin.201400001).
- [47] I. Gil, J. Mendiguren, L. Galdos, E. Mugarra, E. S. de Argandoña],  
527 Influence of the pressure dependent coefficient of friction on deep drawing  
528 springback predictions, *Tribology International* 103 (2016) 266 – 273.  
529 doi:<https://doi.org/10.1016/j.triboint.2016.07.004>.

- [48] X. Ma, M. [de Rooij], D. Schipper, A load dependent friction model  
531 for fully plastic contact conditions, *Wear* 269 (11) (2010) 790 – 796.  
532 doi:<https://doi.org/10.1016/j.wear.2010.08.005>.
- [49] T. Maeno, K. Osakada, K. Mori, Reduction of friction in compression of plates by load  
534 pulsation, *International Journal of Machine Tools and Manufacture* 51 (7) (2011) 612 –  
535 617. doi:<https://doi.org/10.1016/j.ijmachtools.2011.03.007>.
- [50] N. yu Ben, Q. Zhang, D. an Meng, M. gyu Lee, Analysis of real contact  
537 area and re-lubrication in oscillating bulk forming process by corrosion  
538 method, *Journal of Materials Processing Technology* 253 (2018) 178 – 194.  
539 doi:<https://doi.org/10.1016/j.jmatprotec.2017.10.044>.
- [51] N. yu Ben, Q. Zhang, H. Choi, K. Bandyopadhyay, M.-G. Lee, Experimental  
541 and finite element analysis on oscillating cold forming in consideration of nonlinear  
542 loading-unloading-reloading behavior, *Journal of Manufacturing Processes* 36 (2018) 520  
543 – 534. doi:<https://doi.org/10.1016/j.jmapro.2018.10.043>.
- [52] Astm e112-13, standard test methods for determining average grain size, astm  
545 international, Tech. rep., ASTM International, West Conshohocken, PA (2013).  
546 doi:10.1520/E0112-13.